Control of Distributed Photovoltaic Inverters for Frequency Support and System Recovery

H. Dehghani Tafti, G. Konstantinou, J. Fletcher, L. Callegaro, G. G. Farivar and J. Pou

Cite as:
H. Dehghani Tafti, G. Konstantinou, J. Fletcher, L. Callegaro, G. G. Farivar and J. Pou, "Control of Distributed Photovoltaic Inverters for Frequency Support and System Recovery," in *IEEE Trans. Power Electron.*, doi: 10.1109/TPEL.2021.3122180.

IEEE Transactions on Power Electronics, doi: 10.1109/TPEL.2021.3122180

This article has been accepted for publication in a future issue of this journal, but has not been fully edited. Content may change prior to final publication. Citation information: DOI 10.1109/TPEL.2021.3122180, IEEE Transactions on Power Electronics

Control of Distributed Photovoltaic Inverters for Frequency Support and System Recovery

Hossein Dehghani Tafti, *Senior Member IEEE*, Georgios Konstantinou, *Senior Member IEEE*, John E. Fletcher, *Senior Member IEEE*, Leonardo Callegaro, *Member IEEE*, Glen G. Farivar, *Senior Member IEEE* and Josep Pou, *Fellow, IEEE* .

***Abstract*—Replacing conventional synchronous generator-based power plants with inverter-based renewable energy resources results in a reduction of the inertia in power systems. To sustain the security and reliability of these low-inertia power systems, frequency support is increasingly required in new standards for grid-connected renewable energy resources, especially distributed photovoltaic (DPV) systems. This paper proposes a frequency droop-based control in DPV inverters to improve frequency response in power grids with high penetration of renewable energy resources. A predefined power reserve is kept in the DPV inverter, using flexible power point tracking. The proposed algorithm uses this available power reserve to support the grid frequency. Furthermore, a recovery process is proposed to continue injecting the maximum power after the disturbance, until frequency steady-state conditions are met. The positive inertia using the proposed recovery mode, leads to recovery of the frequency in a shorter period. A composite load model of a distribution feeder, including DPV, is developed to assess the effectiveness of the proposed frequency support algorithm in power systems with high penetration of DPV inverters. The dynamic performance of the proposed frequency support algorithm with over-frequency and under-frequency events is also evaluated experimentally.**

***Index Terms*—Active power control, distributed photovoltaic systems, flexible power point tracking, frequency support, inertia provision, low inertia power system.**

Manuscript received March 07, 2021; revised June 27, 2021 and September 22, 2021; accepted October 16, 2021. This work is partly funded under the project 'UNSW Addressing Barriers to Efficient Renewable Integration' funded by the Australian Renewable Energy Agency (ARENA), grant number G00865. The publication is also partially funded by the Future Battery Industries Cooperative Research Centre (www.fbicrc.com.au) as part of the Australian Government's CRC Program, which supports industry-led collaborations between industry, researchers and the community. Further information about the CRC Program is available at www.business.gov.au. The work was also partially supported by the Singapore Ministry of Education Academic Research Fund Tier 1 under Grant No: 2019-T1-001-168 (RG 80/19). The work of Leonardo Callegaro was supported by Macquarie University ECR Enabling Scheme 2021, under Grant 168590913. *(Corresponding author: Hossein Dehghani Tafti.)*

H. D. Tafti is with the Department of Electrical, Electronic and Computer Engineering, University of Western Australia, Crawley WA 6009, Australia (e-mail: hossein002@e.ntu.edu.sg).

G. Konstantinou and J. E. Fletcher are with the School of Electrical Engineering and Telecommunications, University of New South Wales, Sydney, NSW 2052, Australia (e-mail: g.konstantinou@unsw.edu.au, john.fletcher@unsw.edu.au).

L. Callegaro is with the School of Engineering, Macquarie University, Sydney, NSW 2109, Australia (e-mail: leonardo.cllgr@gmail.com).

G. G. Farivar is with Energy Research Institute, Nanyang Technological University, Singapore 639798, Singapore (e-mail: gh_farivar@hotmail.com).

J. Pou is with the School of Electrical and Electronic Engineering, Nanyang Technological University, Singapore 639798, Singapore (e-mail: josep.pou@ieee.org).

I. Introduction

SYNCHRONOUS generator-based power plants contain natural mass inertia, which provides frequency response under any load change or contingency in the power system. Massive integration of inverter-based renewable energy systems has been displacing conventional generating units leading to low-inertia power systems [1], [2]. Several new challenges about reliability and security exist in these systems. Accordingly, new standards and grid codes require frequency support for distributed energy storage inverters [3], [4]. For instance, the new version of AS/NZS 4777.2:2020 requires distributed hybrid photovoltaic (PV) and battery inverters to increase the output power, if frequency decreases below a threshold, based on a predefined droop characteristic.

Several solutions based on different types of renewable energy resources for frequency support have been proposed in the literature [5]–[10]. The integration of energy storage in the power systems is a promising solution, but an expensive one [6], [7]. One of the alternative solutions to grid frequency support is to use the available inertia in large wind power plants [8]–[10]. Another alternative is to use synchronous condensers [11], but they have high installation costs and can only be used for grid voltage and frequency improvement.

Installation of distributed photovoltaic (DPV) inverters is growing rapidly worldwide, because of government support, high electricity costs, and improving technology. DPV inverters are mainly installed in residential locations and are scarcely visible to power system operators. Their output active/reactive power is typically not controlled in real-time by grid operators. As an example, South Australia has 33% of dwellings with rooftop DPV systems. in October 2020, the amount of solar power generated was enough to meet 100% of South Australia needs [12]. Accordingly, frequency support using power reserve control in PV systems is becoming one of the promising solutions in future grids with high penetration of DPV inverters. Unlike the conventional maximum power point tracking (MPPT) algorithms, an intended amount of power reserve is kept in the PV system [13], [14]. This amount of power reserve can be used during under-frequency conditions, to improve the grid frequency response.

Several solutions on the flexible control of DPV inverters output power have been proposed in the literature [15]–[17]. The focus of these studies is on the calculation of the PV voltage reference for a given power reference. However, they do not provide a solution for providing the power reserve to

This article has been accepted for publication in a future issue of this journal, but has not been fully edited. Content may change prior to final publication. Citation information: DOI 10.1109/TPEL.2021.3122180, IEEE Transactions on Power Electronics

support the grid frequency in DPV inverters. To provide a power reserve in PV systems various algorithms are available in the literature [18], [19]. These algorithms either measure the maximum power point (MPP) [18], [20] or estimate it based on the PV panel characteristics [14], [21]. The focus of these studies is on the power converter control to provide a predefined amount of power reserve in the PV system, but they do not provide a detailed solution for how to use the power reserve to support and restore the grid frequency.

The impact of mandatory frequency support in large-scale PV systems is studied in [13]. In large-scale PV systems, the power reference is regulated by the power system operator, based on the grid frequency. Such solutions are impractical for DPV inverters, which operate remotely and without communications with the grid operators. A combined PV and wind system is presented in [22], which uses the forecast data of the PV and wind power to optimize the power extraction from the two systems to provide frequency support. However, there is no available solution in the literature that provides inertia provision and system recovery in DPV inverters.

To tackle this shortcoming, this paper proposes an algorithm for grid frequency support and power systems recovery in DPV inverters to improve the grid frequency response. The proposed solution regulates an intended amount of power reserve in DPVs using flexible power point tracking (FPPT). The main contributions of this paper can be summarized as:

- To propose an algorithm for applying power reserve in DPV inverters to improve the grid frequency response.
- To propose a recovery operation mode in DPV inverters after the frequency disturbance to achieve faster frequency recovery response time.

A composite load model (CMLD) of a distribution feeder is developed to analyze the effectiveness of the proposed frequency support algorithm in improving the grid frequency response in power systems with high penetration of renewable energy resources. The dynamic performance of the proposed algorithm is also evaluated experimentally with under- and over-frequency disturbances.

The remaining parts of the paper are structured as follows: The theory and detailed implementation of the proposed frequency support algorithm is provided in Section II. A comparison of the effectiveness of the proposed frequency support approaches in improving the frequency response to the conventional MPPT algorithm is provided in Section III. Experimental results are included in Section IV, and conclusions of the paper are outlined in Section V.

II. Proposed Frequency Support and System Recovery Approach

This section outlines the details of the proposed frequency support approach in DPV inverters to support the grid frequency. The control diagram of the proposed approach in a two-stage DPV inverter is illustrated in Fig. 1(a). A similar control algorithm can also be implemented in a single-stage DPV inverter. The grid frequency f_g is calculated using a conventional frequency measurement, e.g., phase-lock-loop (PLL) [23]. The calculated frequency f_g is then given as the input to

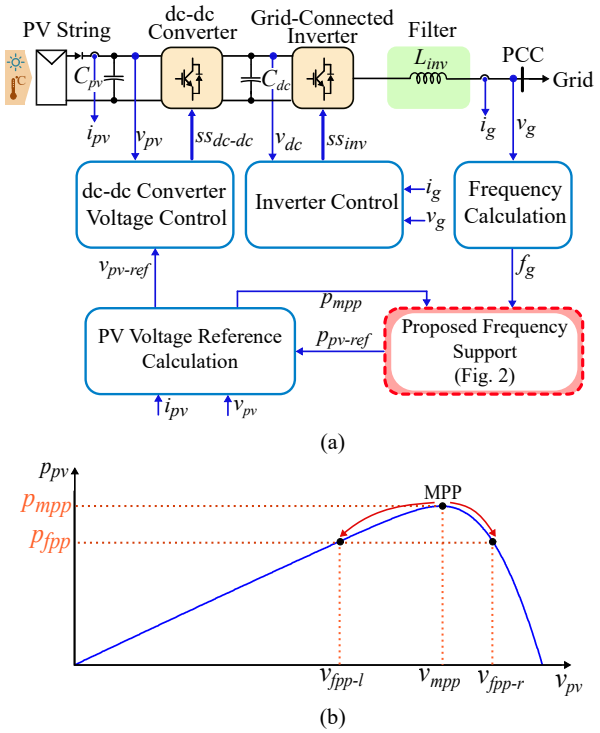

Fig. 1. (a) Control diagram of the proposed frequency support approach, and (b) basics of flexible power point tracking.

the proposed frequency support block. A conventional inverter controller is implemented to regulate the dc-link voltage v_{dc} to its reference value and inject the extracted power from the PV string to the grid [24].

The proposed frequency support algorithm calculates the PV power reference $p_{pv\text{-}ref}$, based on the grid frequency. The details of this block are provided in the following subsections. An adaptive voltage step-based algorithm for calculating the PV voltage reference $v_{pv\text{-}ref}$ based on [24] is used, which result in fast dynamics and low power oscillations at steady-state. A conventional controller is also implemented to regulate the PV voltage v_{pv} to its reference value [24].

The following subsections describe the details of three approaches (including the proposed one), which can be implemented in the block named as "Proposed Frequency Support Approach" in Fig. 1.

A. Maximum Power Point Tracking

The conventional MPPT approach extracts at all times the maximum power p_{mpp} from PV strings, by operating them at the MPP, as in Fig. 1(b). In this approach, PV power reference $p_{pv\text{-}ref}$ is always set at the nominal maximum power of the PV string in Fig. 1(a). In this case, the "PV Voltage Reference Calculation" block, calculates the voltage corresponding to the MPP v_{mpp} and accordingly, the DPV inverter injects the maximum available power to the grid.

As illustrated in Fig. 2(a), the DPV system operates at MPP within the nominal frequency range. A typical grid frequency waveform before and after a contingency or load change in the system (as an example) is shown in Fig. 2(b). Even though

This article has been accepted for publication in a future issue of this journal, but has not been fully edited. Content may change prior to final publication. Citation information: DOI 10.1109/TPEL.2021.3122180, IEEE Transactions on Power Electronics

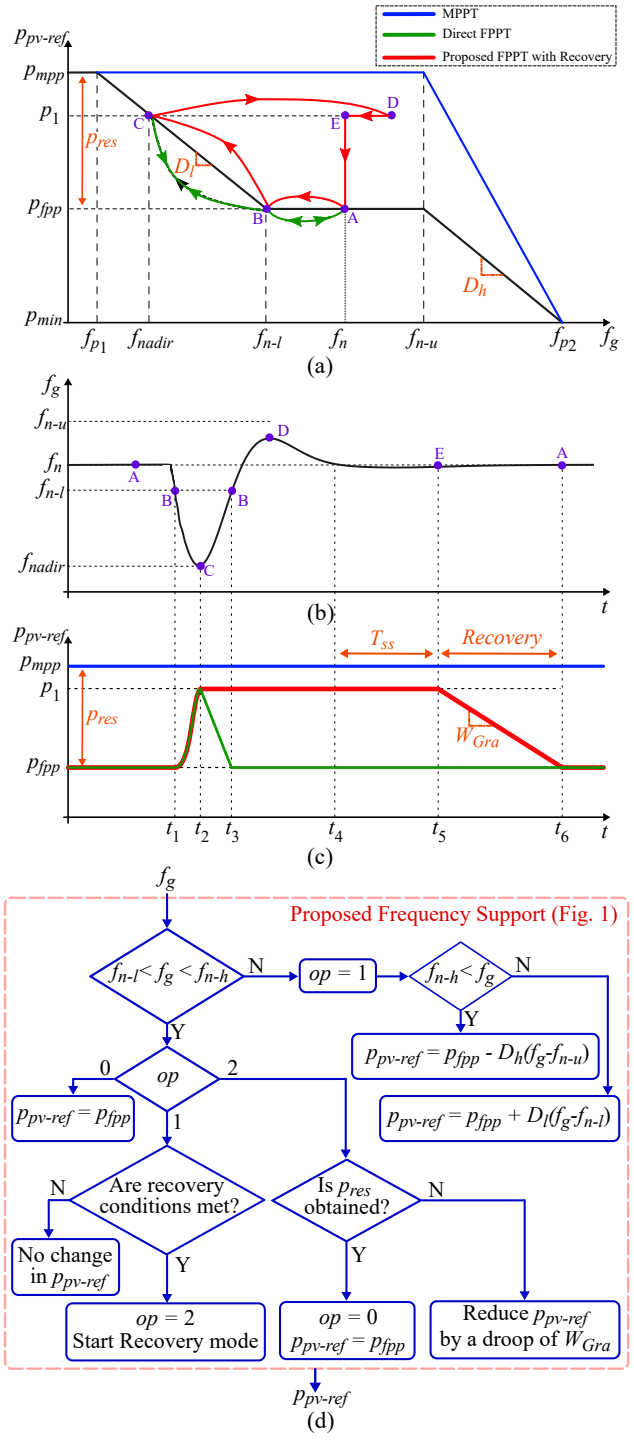

Fig. 2. Proposed frequency support and recovery approach in distributed photovoltaic inverters: (a) Frequency-Watt curve of the proposed approach, (b) a typical grid frequency waveform under sudden load changes or contingencies, (c) DPV inverter output power, and (d) flowchart of the proposed approach.

the grid frequency deviates from its nominal value between t_1 and t_4, the DPV inverter with the conventional MPPT approach injects maximum available PV power p_{mpp} to the grid, as depicted in Fig. 2(c). In this strategy, DPV inverters do not contribute to the frequency support. During periods of peak power generation from DPV inverters (e.g., the middle of the day), these inverter-based generation systems supply a high portion of the load demand. Subsequently, during a contingency, the power system can face several challenges related to security and frequency response due to the low inertia.

B. Direct Flexible Power Point Tracking

Fig. 2 shows the operation principle of the direct FPPT algorithm. If the grid frequency f_g is within the upper and the lower limits of the nominal value, shown as $f_{n\text{-}l}$ and $f_{n\text{-}u}$, respectively, (i.e. $f_{n\text{-}l} < f_g < f_{n\text{-}u}$), the DPV inverter operates at a reduced power reference p_{fpp}, to keep an intended amount of power reserve p_{res} in the system. The operation point under such condition can be selected as in the right- or left-side of the MPP, depicted in Fig. 1(b). Different values shall be selected for the controller parameters to obtain a similar dynamic with operation in the left- or right-side of the MPP [24]. Before t_1, f_g is equal to its nominal value f_n. Therefore, the DPV inverter injects p_{fpp} to the grid during this period.

If f_g reduces below the threshold value of $f_{n\text{-}l}$, the PV output power increases based on the droop curve between points B and C, and according to the frequency nadir f_{nadir}, as demonstrated in Fig. 2(a). Under this condition, the operation point moves from A to C and the output power increases to p_1, corresponding power to f_{nadir}, as illustrated in Fig. 2(c). This operation of the DPV inverter provides virtual positive inertia for the power system under a frequency disturbance. Such virtual positive inertia from DPV inverters increases the system inertia and leads to an improved frequency response in power systems with high penetration of DPV inverters.

In the direct FPPT approach, the DPV output power is set based on the instantaneous grid frequency f_g and the predefined frequency-Watt curve. In the interval between t_2 and t_3, in which f_g increases from its minimum f_{nadir} towards its nominal, the DPV output power also decreases from p_1 to p_{fpp}, corresponding to the droop curve. Afterward, f_g remains within the nominal threshold range and subsequently the DPV power is equal to p_{fpp}.

The direct FPPT approach supports the grid frequency at the beginning of the disturbance (before t_2) by adding a virtual positive inertia to the system. However, after this time instance, the DPV power reduces, which emulates a negative virtual inertia to the power system. This means that the conventional power plants require to compensate for the full change of the load, which leads to an increase of the frequency recovery response time. However, with the inclusion of a recovery mode, the DPV inverters compensate for a portion of the load change, which means the conventional power plants require to compensate for a smaller value of the load change. Accordingly, the inclusion of recovery mode, can result in a faster frequency recovery time. The details of the proposed recovery mode are provided in the following subsection.

C. Proposed Flexible Power Point Tracking with Recovery

Based on the aforementioned discussion about the disadvantage of disregarding the recovery in the direct FPPT approach,

This article has been accepted for publication in a future issue of this journal, but has not been fully edited. Content may change prior to final publication. Citation information: DOI 10.1109/TPEL.2021.3122180, IEEE Transactions on Power Electronics

this section provides details of the proposed FPPT with recovery approach. As illustrated in Fig. 2(a), the operation of both direct FPPT and the proposed FPPT with recovery approaches before frequency nadir (before t_2) are the same. The DPV output power increases from p_{fpp} to p_1, corresponding to the grid minimum frequency f_{nadir} at the beginning of the disturbance.

In the proposed FPPT with recovery approach, after t_2, the DPV power remains at p_1 (corresponding to f_{nadir}) until the following conditions are met:

- The grid frequency f_g remains within the nominal upper and lower threshold values ($f_{n\text{-}l} < f_g < f_{n\text{-}u}$) for a predefined period T_{ss}.
- The rate-of-change-of-frequency (RoCoF) for a period of T_{ss} is smaller than the predefined threshold $RoCoF_{th}$ ($RoCoF < RoCoF_{th}$).

In the example in Fig. 2, these conditions are satisfied between t_4 and t_5. Subsequently, the DPV inverter operation changes to the recovery mode.

During the recovery period, the DPV power reduces from p_1 to p_{fpp} with the defined power ramp rate W_{Gra}. The value of W_{Gra} is imposed by corresponding standards. For example, AS/NZS 4777.2:2020 imposes 16.67% of the rated power per minute [4].

The proposed FPPT with recovery enhances the grid frequency response by avoiding negative virtual inertia, which is enforced to the power system in the direct FPPT approach. In this way, DPV inverters compensate some percentage of the load change or generation lost in the system during and after the grid frequency disturbance. Accordingly, the conventional power plants require compensating for a smaller portion of the power. In other words, the proposed approach results in lower power requirements from rotating synchronous generators during frequency events, therefore demanding less inertia to be available in the grid. In this case, due to the fast response from DPV inverters, the grid frequency can recover in a shorter period.

A flowchart for the implementation of the proposed FPPT approach with recovery is illustrated in Fig. 2(c). Three operation modes are considered:

- *op* = 0: This mode relates to steady-state operation of the system, in which frequency is within the nominal range and the DPV system reserves p_{res} in the system.
- *op* = 1: This operation mode is activated after detection of a disturbance, in which the DPV power is increased based on the frequency droop gain. Based on the frequency nadir, it may operate at the MPP under this mode. The DPV system remains in this mode, until the recovery conditions are satisfied.
- *op* = 2: This operation mode is enabled after the recovery conditions are met with the DPV system. In this operation mode, the DPV system decreases the power, based on the predefined power ramp rate.

As shown in Fig. 2(c), if the frequency goes out of the nominal range, the operation mode is set to $op = 1$. Depending on the frequency value, the DPV output power either increases or decreases based on the defined droop values. Under $op = 1$, the DPV power stays on the calculated reference value based on the frequency nadir and the conditions for recovery are regularly checked. After satisfying the recovery conditions, the recovery mode $op = 2$ is commenced. Finally, once, p_{res} is obtained in the DPV system, the operation mode switches to $op = 0$.

$$\begin{aligned} R_r(t) &= \frac{dP_{\mathrm{pv}}}{dt} = \frac{\Delta P_{\mathrm{pv}}}{T_{\mathrm{RRM}}} \\ &= \frac{P_{\mathrm{pv}}(t) - P_{\mathrm{pv}}\left(t + T_{\mathrm{RRM}}\right)}{T_{\mathrm{RRM}}} \\ &= \frac{P_{\mathrm{pv}}(t) - P_{\mathrm{pr}}\left(t + nT_s\right)}{nT_s} \end{aligned} \tag{1}$$

TABLE I
FREQUENCY-WATT CURVE PARAMETERS

Parameter	Value
Nominal frequency, f_n	50 Hz
Nominal frequency upper threshold, $f_{n\text{-}u}$	50.25 Hz
Nominal frequency lower threshold, $f_{n\text{-}l}$	49.75 Hz
Over frequency power injection limit, f_{p2}	52 Hz
Under frequency maximum power limit, f_{p1}	49 Hz
Power reserve, p_{res}	$0.2p_{mpp}$ (20%)

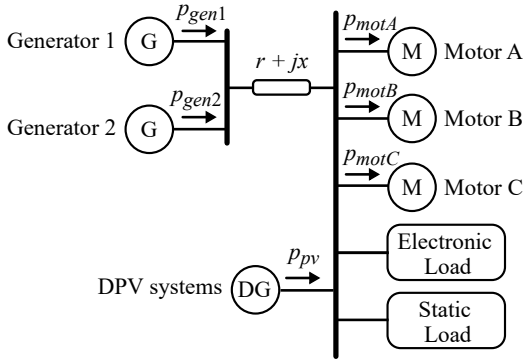

Fig. 3. Diagram of the composite load model of a distribution feeder.

III. RESULTS AND DISCUSSION

A CMLD has been developed to investigate the effectiveness of the proposed frequency support approach in improving the grid frequency response. The selected parameters for the frequency-Watt curve in Fig. 2(a) are listed in Table I. A detailed description of the simulated CMLD is provided in the following subsection. Two events, leading to frequency disturbances are simulated: 1) Load step change, and 2) generator fault, and details are provided in the subsequent subsections.

A. Composite Load Model

Exhaustive international work has paved the way toward the development of more precise CMLDs for power system dynamic simulations. Recently, the western electricity coordinating council (WECC) proposed a generic CMLD that

This article has been accepted for publication in a future issue of this journal, but has not been fully edited. Content may change prior to final publication. Citation information: DOI 10.1109/TPEL.2021.3122180, IEEE Transactions on Power Electronics

TABLE II
PARAMETERS OF THE SIMULATED COMPOSITE LOAD MODEL

Component	Nominal Power (MVA)	Proportion of the Load (%)	Inertia (s)
Generator 1	2	-	2
Generator 2	0.5	-	1
Motor A	0.9	37.5	0.1
Motor B	0.6	25	0.5
Motor C	0.5	20.8	0.1
Electronic load	0.15	6.3	-
Static load	0.25	10.4	-
DPV system	1.5	-	-

includes a representation of the distribution feeder, and the aggregate behavior of various loads and DERs connected in distribution systems [25]–[27]. A diagram of the WECC CMLD for a distribution feeder is depicted in Fig. 3. The CMLD is employed in this study to verify the effectiveness of the proposed approach on frequency response, because it includes the inertia from generators as well as motor loads. However, the inertia from motor loads connected to a distribution feeder is typically ignored in similar studies.

A short description of the details of each load component of the CMLD is provided below. Some of the important parameters of each component of the simulated CMLD are also provided in Table II.

- *Motor A*: This motor represents an aggregation of three-phase induction motors with low inertia ($H = 0.1\,\text{s}$) that are usually installed in industrial premises to drive constant torque loads.
- *Motor B*: This motor is a representation of aggregated three-phase induction motors with high inertia ($H = 0.25$-$1\,\text{s}$). The load torque of such motor is proportional to the square of the speed. This motor represents the motors found in commercial ventilation fans and air handling systems.
- *Motor C*: The aggregation of commonly found commercial water circulation pumps is represented with this motor with low inertia ($H = 0.1$-$0.2\,\text{s}$).
- *Electronic Load*: This type of load represents electronic-based loads with constant active and reactive power for a range of grid voltage values.
- *Static loads*; This component is modeled using polynomial equations, which relate the load to the voltage and frequency. This load represents other available types of loads in the distribution system, which are not mentioned above.

Generators 1 and 2 represent two synchronous generator-based power plants with different nominal powers and inertia parameters. The distributed generator (DG) represents multiple residential DPV systems connected to the distribution feeder. The power rating of this system is chosen as $1.5\,\text{MW}$ to represent a relatively high penetration of DPV inverters in the system.

Remark: The CMLD also includes *Motor D*, that represents single-phase motors and is not implemented in this study.

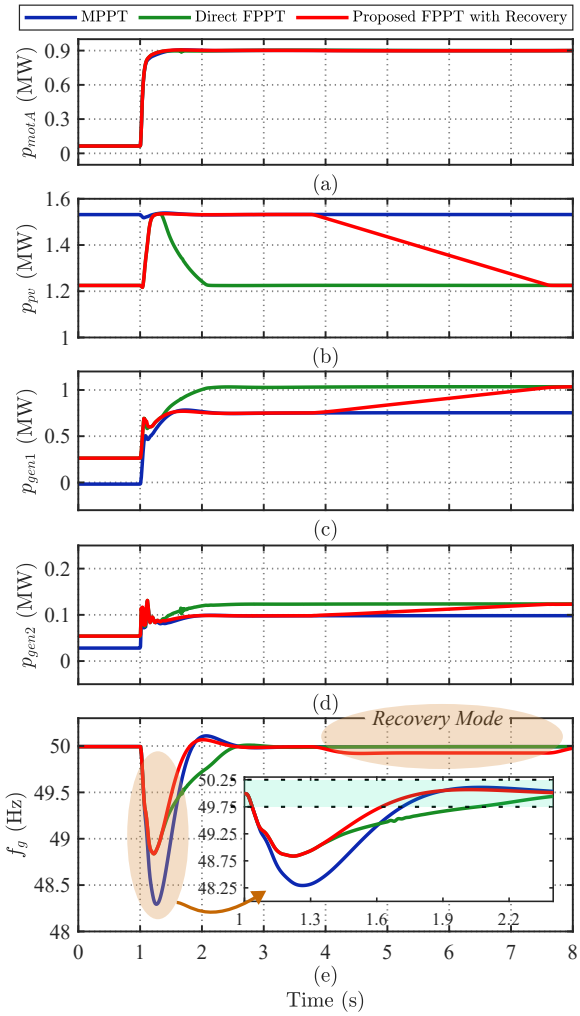

Fig. 4. Simulation results - *Load step change*: Comparison of the grid frequency response with the proposed frequency support approaches under load step change condition: (a) Motor A load power; (b) DPV system output power; (c) Generator 1 output power; (d) Generator 2 output power; and (e) grid frequency.

B. Load Step Change

A step increase in the load of Motor A is simulated in this case study and results are illustrated in Fig. 4. Before $t = 1\,\text{s}$, the load of Motor A $p_{motA} = 0.05\,\text{MW}$. Under this condition, the DPV inverter with conventional MPPT approach injects the maximum PV power ($1.5\,\text{MW}$), while it injects 80% of the available PV power with the direct FPPT and the proposed FPPT with recovery approaches. The grid frequency f_g is regulated to its nominal value of $50\,\text{Hz}$ during this period.

As depicted in Fig. 4(a), Motor A load increases in a step wise manner from $0.05\,\text{MW}$ to $0.9\,\text{MW}$ at $t = 1\,\text{s}$. Such a step load change decreases the grid frequency, shown in Fig. 4(e). The $RoCoF$ value for all three approaches is similar at the beginning of the frequency disturbance, as the available inertia from generators and motors is the same in the three approaches.

During the frequency disturbance, the conventional MPPT algorithm continues to inject the maximum power from the PV

This article has been accepted for publication in a future issue of this journal, but has not been fully edited. Content may change prior to final publication. Citation information: DOI 10.1109/TPEL.2021.3122180, IEEE Transactions on Power Electronics

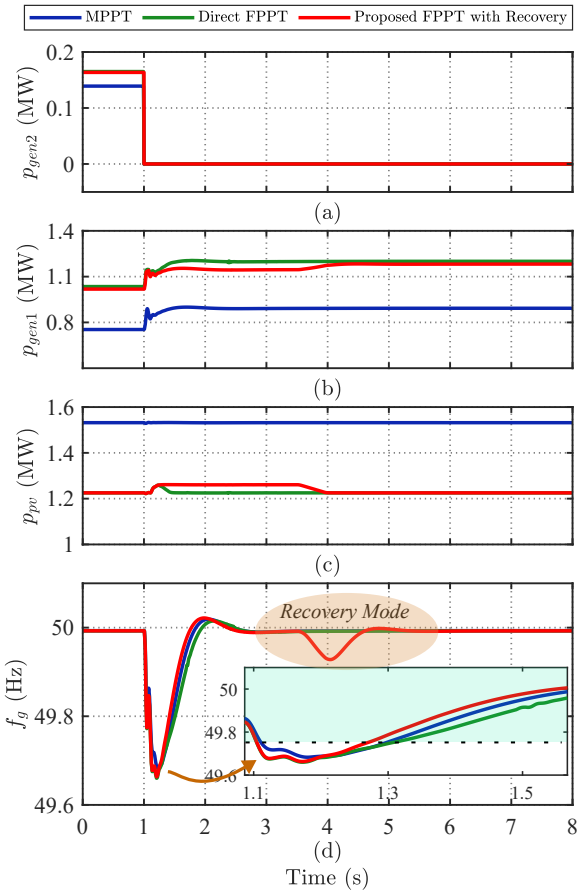

Fig. 5. Simulation results - *Generator fault*: Comparison of the grid frequency recovery with the proposed frequency support approaches under generator fault condition: (a) Generator 2 output power; (b) Generator 1 output power; (c) DPV system output power; and (d) grid frequency.

system and the DPV inverter is not involved in the frequency support. Accordingly, the frequency nadir is $f_{nadir} = 48.3\,\text{Hz}$. Fig. 4(b) shows that the DPV output power increases using the direct FPPT approach from the power reserve value before the disturbance to the maximum of $1.5\,\text{MW}$ after $t = 1\,\text{s}$. It is clear from Fig. 4(e) that the frequency nadir is improved in both direct FPPT and proposed FPPT with recovery approaches, compared to the conventional MPPT approach. The frequency nadir is improved to $48.8\,\text{Hz}$ using these two approaches.

The frequency response in both direct FPPT and proposed FPPT with recovery approaches at the beginning of the frequency disturbance (between $t = 1\,\text{s}$ and $t = 1.6\,\text{s}$) is the same. After $t = 1.6\,\text{s}$, the direct FPPT approach reduces the DPV power based on the frequency-Watt curve in Fig. 2(a) and the frequency recovers to the nominal range (between $f_{n\text{-}l}$ and $f_{n\text{-}l}$) at $t = 2.1\,\text{s}$. Simultaneously, for the proposed FPPT with recovery approach, Fig. 4(e) reveals that the frequency recovers to the nominal range in a shorter period at $t = 1.6\,\text{s}$. This result highlights the advantage of the proposed approach with recovery mode to recover the grid frequency to the nominal range in a shorter period. The longer response time in the direct FPPT approach is because the two generators (in Fig. 3) require to compensate for the load increase and the decrease of DPV power. However, in the proposed FPPT with recovery approach, generators are only required to compensate for the load increase, as DPV systems continue generating maximum power after $t = 1.76\,\text{s}$.

The recovery mode of the proposed FPPT with recovery approach starts at $t = 3.9\,\text{s}$, as shown in Fig. 4(b). The DPV power reduces from $1.5\,\text{MW}$ (i.e., the maximum power p_{mpp}) with the defined ramp rate. The power reaches the power reserve value at $t = 7.5\,\text{s}$. There is a small drop in the grid frequency during the recovery mode. The power ramp rate is chosen in such a way that the frequency remains within the nominal threshold range. As shown in Figs. 4(c) and (d), the output powers of Generators 1 and 2 increase during the recovery mode to compensate for the reduction of power from the DPV inverter.

C. Generator Fault

To investigate the effectiveness of the proposed frequency support approaches in grid frequency support under grid contingencies, a sudden failure of Generator 2 is analyzed in this case study, and results are illustrated in Fig. 5. The failure happens at $t = 1\,\text{s}$ and the output power of Generator 2 drops to zero, as depicted in Fig. 5(a). The DPV inverter output power increases in direct FPPT and proposed FPPT with recovery approaches, following the frequency-Watt curve in Fig. 2(a). This increase in the output power helps to limit the frequency nadir f_{nadir} in these methods. Furthermore, Fig. 5(d) shows that the proposed FPPT with recovery approach helps to recover the frequency in a shorter period, compared to the direct FPPT approach.

A summary of frequency recovery results for various simulation case studies is provided in Table III. It is seen that under most conditions, the proposed FPPT with recovery approach results in an improved frequency nadir, compared to the conventional MPPT algorithm. It also reduces the frequency recovery response time, compared to the conventional approaches. It should be noted that the amount of frequency nadir improvement or frequency recovery response time depends on the setting of the parameters of the algorithm and can be optimally designed for an specific power system.

IV. Experimental Results

The performance of the proposed frequency support approaches is evaluated experimentally on a 2.5-kW two-stage DPV system, as shown in Fig. 1. The dc-dc boost converter and grid-connected inverter consist of Semikron SKM145GB176D 1700V IGBT modules. The grid is simulated using a Regatron TCACS 4-quadrant grid simulator and the PV is emulated using a Regatron TopCon Quadro programmable dc power supply. The proposed frequency support approaches are implemented on the dc-dc converter and the proposed controller and protection functions of the converter are implemented in a dSPACE 1006 platform. A picture of the experimental setup is illustrated in Fig. 6 and the parameters of the converter are given in Table IV.

TABLE III
SUMMARY OF FREQUENCY RECOVERY RESULTS

	Frequency nadir (Hz)			Frequency response time (s)		
	MPPT	Direct FPPT	**Prop. FPPT with Rec.**	MPPT	Direct FPPT	**Prop. FPPT with Rec.**
Motor A step load change from 0.05 MW to 0.3 MW	49.4	49.5	**49.5**	0.7	0.8	**0.6**
Motor A step load change from 0.05 MW to 0.6 MW	48.8	49.2	**49.2**	0.8	1.1	**0.6**
Motor A step load change from 0.05 MW to 0.9 MW	48.3	48.8	**48.8**	0.7	1.6	**0.6**
Generator 2 fault	49.7	49.7	**49.7**	0.7	0.7	**0.55**

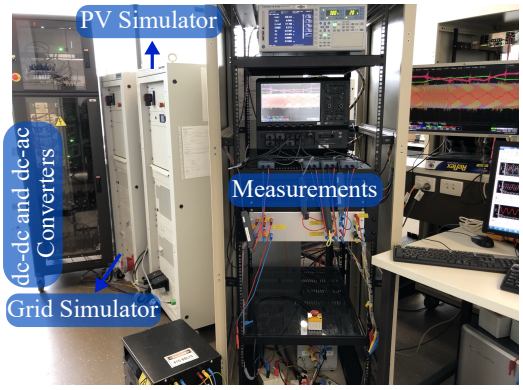

Fig. 6. Experimental setup.

TABLE IV
EXPERIMENTAL PARAMETERS

Parameter	Value
PV string maximum power, p_{mpp}	2.5 kW
PV string *MPP* voltage, v_{mpp}	275 V
PV string capacitor, C_{pv}	1.1 mF
Grid voltage (line-neutral, rms), $v_{g\text{-}ln}$	110 V
Grid frequency, f	50 Hz
Grid connection inductor filter, L_f	9 mH

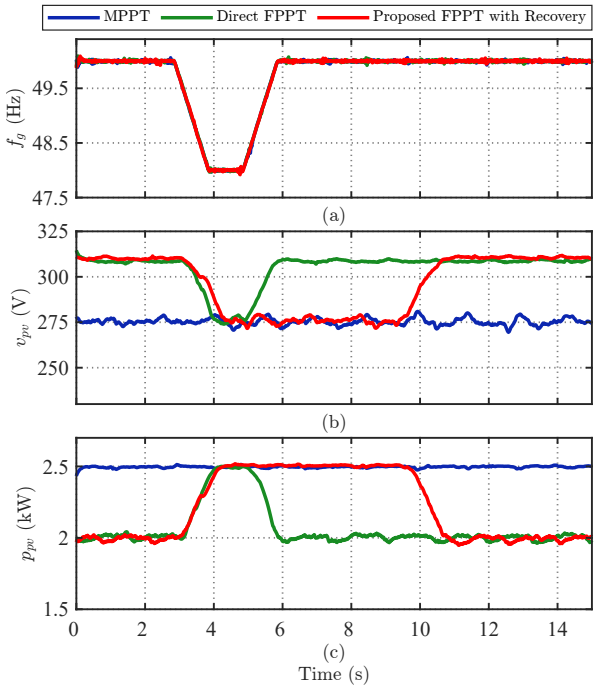

Fig. 7. Experimental results - *Case I*: Performance of the proposed frequency support approaches with grid under-frequency condition: (a) Grid frequency; (b) PV voltage; and (c) PV power.

The proposed controller is evaluated under two different cases corresponding to under-frequency conditions (*Case I* - Fig. 7) and over-frequency condition (*Case II* - Fig. 8).

Case I: In this experimental case study, an under-frequency event is emulated in the grid and the performance of the proposed inertia provision approaches are shown in Fig. 7. As illustrated in Fig. 7, the grid frequency f_g is at the nominal value (50 Hz) before $t = 3$ s. During this period, the direct FPPT and proposed FPPT with recovery approaches extract 2 kW power from the DPV system, which equals to 80% of the maximum available power from the DPV system ($p_{mpp} = 2.5$ kW). Simultaneously, the conventional MPPT algorithm extracts the maximum power from the DPV system. At $t = 3$ s, the grid frequency drops linearly from 50 Hz to 48 Hz in a period of 1 s ($RoCoF = 2$ Hz/s). The conventional MPPT algorithm remains at the maximum power point and continues to inject 2.5 kW power to the grid. However, the direct FPPT and proposed FPPT with recovery approaches increase the inverter output power to the maximum available DPV power as shown in Fig. 7(c). As demonstrated in Section III, such an increase in DPV output power under grid under-frequency disturbances results in an improvement of the grid frequency response.

The grid frequency f_g returns to its nominal value between $t = 5$ s and $t = 6$ s. The direct FPPT approach reduces the DPV output power instantaneously based on the frequency-Watt curve, while the proposed FPPT with recovery approach continues injecting the maximum power to the grid during this condition. As explained in Section III, the proposed FPPT with recovery approach leads to a better frequency response compared to the direct FPPT approach. In the proposed FPPT with recovery approach, the DPV output power decreases

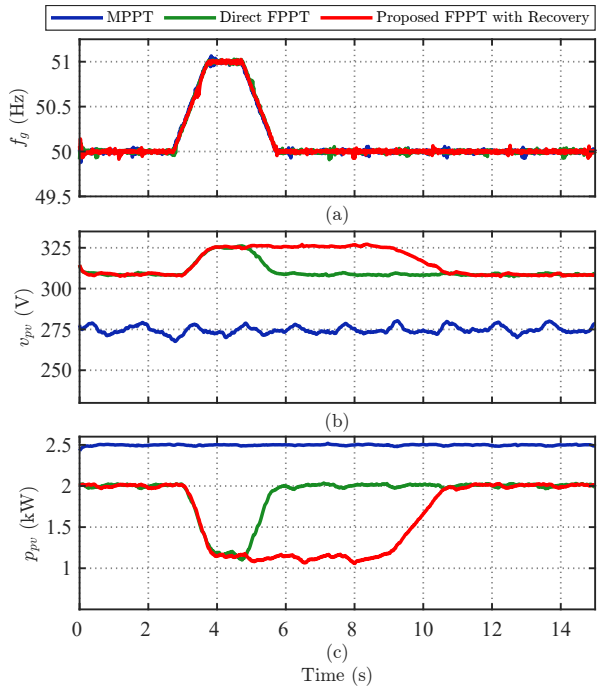

Fig. 8. Experimental results - *Case II*: Performance of the proposed frequency support approaches with grid over-frequency condition: (a) Grid frequency; (b) PV voltage; and (c) PV power.

based on the defined power ramp rate after the conditions for the recovery mode are met, at $t = 10\,\mathrm{s}$. Afterward, the DPV output power remains at 80% of the maximum available power.

Case II: In this case study an over-frequency disturbance has been emulated and results are shown in Fig. 8. The grid frequency f_g increases from $50\,\mathrm{Hz}$ to $51\,\mathrm{Hz}$ between $t = 3\,\mathrm{s}$ and $t = 4\,\mathrm{s}$ with $RoCoF = 1\,\mathrm{Hz/s}$. During this period, the proposed FPPT with recovery approach reduces the DPV power from $2\,\mathrm{kW}$ to $1.1\,\mathrm{kW}$ based on the defined frequency-Watt curve. The DPV power remains at this value, until the conditions for the recovery mode are met. Afterward, the DPV power increases based on the predefined power ramp rate.

V. Conclusion

An FPPT algorithm with recovery approach in DPV systems has been proposed for grid frequency support. The proposed approach keeps a predefined power reserve in each DPV system and uses this amount of power reserve during grid under-frequency disturbances to improve the grid frequency response. The proposed recovery mode with the FPPT approach helps to recover the grid frequency in a shorter time. The integration of the proposed frequency support and recovery approach in the composite load model of a distribution feeder, has verified its effectiveness in increasing the minimum frequency (frequency nadir) under load step increase and grid contingencies. It also reduced the frequency recovery response time of the system by providing a positive virtual inertia. The experimental tests verify dynamic performance of the proposed frequency support approaches with under-frequency and over-frequency disturbances.

References

[1] Y. Liu, S. You, J. Tan, Y. Zhang, and Y. Liu, "Frequency response assessment and enhancement of the U.S. power grids toward extra-high photovoltaic generation penetrations-An industry perspective," *IEEE Trans. Power Sys.*, vol. 33, no. 3, pp. 3438–3449, May 2018.

[2] C. Seneviratne and C. Ozansoy, "Frequency response due to a large generator loss with the increasing penetration of wind/PV generation–A literature review," *Renewable and Sustain. Energy Rev.*, vol. 57, pp. 659–668, May 2016.

[3] *IEEE recommended practice for interconnecting distributed resources with Electric Power Systems Distribution Secondary Networks*, IEEE Std 1547.6 (Revision IEEE Std 1547-2003), Apr. 2018.

[4] Australia/New Zealand Standard AS/NZS 4777.2, "Grid-connected PV systems: Design and installation training manual," Dec. 2020. [Online]. Available: https://www.standards.org.au/standards-catalogue/sa-snz/electrotechnology/el-042/as-slash-nzs–4777-dot-2-colon-2020.

[5] E. Serban, M. Ordonez, and C. Pondiche, "Voltage and frequency grid support strategies beyond standards," *IEEE Trans. Power Electron.*, vol. 32, no. 1, pp. 298–309, Jan. 2017.

[6] A. Charalambous, L. Hadjidemetriou, E. Kyriakides, and M. Polycarpou, "A coordinated voltage-frequency support scheme for storage systems connected to distribution grids," *IEEE Trans. Power Electron.*, pp. 1–12, 2020, to be published: 10.1109/TPEL.2020.304603.

[7] W. Liu, G. Geng, Q. Jiang, H. Fan, and J. Yu, "Model-free fast frequency control support with energy storage system," *IEEE Trans. Power Sys.*, vol. 35, no. 4, pp. 3078–3086, Jul. 2020.

[8] M. N. Musarrat, M. R. Islam, K. M. Muttaqi, and D. Sutanto, "Enhanced frequency support from a PMSG-based wind energy conversion system integrated with a high temperature SMES in standalone power supply systems," *IEEE Trans. Appl. Supercond.*, vol. 29, no. 2, pp. 1–6, Mar. 2019.

[9] A. Bidadfar, O. Saborío-Romano, J. N. Sakamuri, N. A. Cutululis, V. Akhmatov, and P. E. Sørensen, "On feasibility of autonomous frequency-support provision from offshore HVDC grids," *IEEE Trans. Power Del.*, vol. 35, no. 6, pp. 2711–2721, Dec. 2020.

[10] E. Rakhshani, A. Perilla, J. L. R. Torres, F. M. Gonzalez-Longatt, T. B. Soeiro, and M. A. M. M. Van Der Meijden, "FAPI controller for frequency support in low-inertia power systems," *IEEE Open Access Journal of Power and Energy*, vol. 7, pp. 276–286, Jul. 2020.

[11] S. Hadavi, M. Z. Mansour, and B. Bahrani, "Optimal allocation and sizing of synchronous condensers in weak grids with increased penetration of wind and solar farms," *IEEE Trans. Emerg. Sel. Topics Circuits Syst.*, pp. 1–1, 2021, to be published: 10.1109/JETCAS.2021.3053554.

[12] Australian Energy Market Operator (AEMO), "South Australian electricity report," Nov. 2020.

[13] B. I. Craciun, T. Kerekes, D. Sera, and R. Teodorescu, "Frequency support functions in large PV power plants with active power reserves," *IEEE Trans. Emerg. Sel. Top. Power Electron.*, vol. 2, pp. 849–858, Dec. 2014.

[14] A. F. Hoke, M. Shirazi, S. Chakraborty, E. Muljadi, and D. Maksimovic, "Rapid active power control of photovoltaic systems for grid frequency support," *IEEE Trans. Emerg. Sel. Topics Power Electron.*, vol. 5, no. 3, pp. 1154–1163, Sep. 2017.

[15] H. D. Tafti, A. I. Maswood, G. Konstantinou, J. Pou, and F. Blaabjerg, "A general constant power generation algorithm for photovoltaic systems," *IEEE Trans. Power Electron.*, vol. 33, no. 5, pp. 4088–4101, May 2018.

[16] A. Kumaresan, H. Dehghani Tafti, K. Nandha Kumar, G. G. Farivar, J. Pou, and T. Subbaiyan, "Flexible power point tracking for solar photovoltaic systems using secant method," *IEEE Trans. Power Electron.*, vol. 36, no. 8, pp. 9419–9429, Aug. 2021.

[17] H. D. Tafti, G. Konstantinou, C. D. Townsend, G. G. Farivar, A. Sangwongwanich, Y. Yang, J. Pou, and F. Blaabjerg, "Extended functionalities of photovoltaic systems with flexible power point tracking: Recent advances," *IEEE Trans. Power Electron.*, vol. 35, pp. 9342–9356, Sep. 2020.

[18] A. Sangwongwanich, Y. Yang, F. Blaabjerg, and D. Sera, "Delta power control strategy for multistring grid-connected PV inverters," *IEEE Trans. Ind. Appl.*, vol. 53, no. 4, pp. 3862–3870, Jul. 2017.

[19] E. I. Batzelis, S. A. Papathanassiou, and B. C. Pal, "PV system control to provide active power reserves under partial shading conditions," *IEEE Trans. Power Electron.*, vol. 33, no. 11, pp. 9163–9175, Nov. 2018.

[20] A. Sangwongwanich, Y. Yang, and F. Blaabjerg, "A sensorless power reserve control strategy for two-stage grid-connected PV systems," *IEEE Trans. Power Electron.*, vol. 32, no. 11, pp. 8559–8569, Nov. 2017.

[21] E. I. Batzelis, G. E. Kampitsis, and S. A. Papathanassiou, "Power reserves control for PV systems with real-time MPP estimation via curve fitting," *IEEE Trans. Sustain. Energy*, vol. 8, no. 3, pp. 1269–1280, Jul. 2017.
[22] S. Camal, A. Michiorri, and G. Kariniotakis, "Optimal offer of automatic frequency restoration reserve from a combined PV/Wind virtual power plant," *IEEE Trans. Power Syst.*, vol. 33, no. 6, pp. 6155–6170, Nov. 2018.
[23] M. S. Reza, F. Sadeque, M. M. Hossain, A. M. Y. M. Ghias, and V. G. Agelidis, "Three-phase PLL for grid-connected power converters under both amplitude and phase unbalanced conditions," *IEEE Trans. Ind. Electron.*, vol. 66, no. 11, pp. 8881–8891, Nov. 2019.
[24] H. D. Tafti, A. Sangwongwanich, Y. Yang, J. Pou, G. Konstantinou, and F. Blaabjerg, "An adaptive control scheme for flexible power point tracking in photovoltaic systems," *IEEE Trans. Power Electron.*, vol. 34, pp. 5451–5463, Jun. 2019.
[25] Western Electricity Coordinating Council (WECC) , "WECC MVWG load model report ver. 1.0," Jun. 2012.
[26] North American Electric Reliability Corporation (NERC), "Technical reference document: Dynamic load modeling," Dec. 2016.
[27] A. Gaikwad, P. Markham, and P. Pourbeik, "Implementation of the WECC composite load model for utilities using the component-based modeling approach," in *Proc. of IEEE/PES Trans. and Distrib. Conf. and Exposition (T&D)*, 2016, pp. 1–5.

Hossein Dehghani Tafti (Senior Member, IEEE) received the B.Sc. and M.Sc. degrees in electrical engineering and power system engineering from the Amirkabir University of Technology, Tehran, Iran, in 2009 and 2011, respectively, and the Ph.D. degree in electrical engineering from Nanyang Technological University, Singapore, in 2018. From January 2018 to April 2020, he was a Research Fellow with Nanyang Technological University, where he was working on the control of photovoltaic systems for grid support. From May 2020 to May 2021, he was a senior research associate with the University of New South Wales, Sydney, Australia, where he worked on modelling and testing of commercial photovoltaic inverters. He is currently a research fellow at the Department of Electrical, Electronic and Computer Engineering, University of Western Australia, Perth, WA. He was the Co-Editor of the book titled Advanced Multilevel Converters and Applications in Grid Integration, published by John Wiley in 2018. His research interest includes the grid-integration of renewable energy sources, in particular, photovoltaics and energy storage and design and control of multilevel power converters.

Georgios Konstantinou (Senior Member, IEEE) received the B.Eng. degree in electrical and computer engineering from the Aristotle University of Thessaloniki, Thessaloniki, Greece, in 2007 and the Ph.D. degree in electrical engineering from UNSW Sydney (The University of New South Wales), Australia, in 2012. From 2013 to 2016, he was a Senior Research Associate with the University of New South Wales, Sydney, NSW, Australia, where he was part of the Australian Energy Research Institute. Since 2017, he has been with the School of Electrical Engineering and Telecommunications, UNSW Sydney, where he is currently a Senior Lecturer. His main research interests include multilevel converters, power electronics in HVDC, renewable energy and energy storage applications. He is an Associate Editor for IEEE Transactions on Power Electronics, IEEE Tranasctions on Industrial Electronics and IET Power Electronics.

John E. Fletcher's (Senior Member, IEEE) research interests include power electronics, machine drives and power conversion with a myriad of applications across a range of sectors. His current research portfolio includes 16 research projects valued at $10.9M, with 20 IP disclosures made in the last 3 years and three philanthropic donations. Demonstrable research impacts include major contributions to new Australian Standards, new regulations and new market participant roles. He is the Head of Energy Systems at UNSW, Energy Institute Industry Engagement Director, EA Accreditation Panel, School Industry Advisory Board, Director of the UNSW Electrifying Lab with a research portfolio in 2021 of $7M.

Leonardo Callegaro (Member, IEEE) received the B.Eng. and M.Eng. (hons.) degrees from the University of Padova, Padova, Italy, in 2004 and 2006, respectively, and the Ph.D. degree from The University of New South Wales, Sydney, Australia, in 2018, all in electrical engineering.

From 2007 to 2014, he mainly worked in the industry sector related to dc power systems for telecommunications and remote area power supplies. From 2018 to 2020 he was a Research Associate with The University of New South Wales. He is currently a Lecturer in Electrical Engineering with Macquarie University, Sydney, Australia. His research interests include control for power electronics in photovoltaic energy systems, electric transportation and grid integration of renewables.

Glen G. Farivar (Senior Member, IEEE) received the B.Sc. degree in electrical engineering from the Nooshirvani Institute of Technology, Babol, Iran, in 2008, the M.Sc degree in power electronics from the University of Tehran, Tehran, Iran in 2011, and PhD in electrical engineering from the University of NSW Australia, Syndey, Australia in 2016. He is currently working as a senior research fellow at the Energy Research Institute, Nanyang Technological University (ERI@N), Singapore. His research interests include renewable energy systems, high power convertors, energy storage, FACTS devices, and hybrid electric vehicles.

Josep Pou (Fellow, IEEE) received received the B.S., M.S., and Ph.D. degrees in electrical engineering from the Technical University of Catalonia (UPC)-Barcelona Tech, in 1989, 1996, and 2002, respectively. In 1990, he joined the faculty of UPC as an Assistant Professor, where he became an Associate Professor in 1993. From February 2013 to August 2016, he was a Professor with the University of New South Wales (UNSW), Sydney, Australia. He is currently a Professor with the Nanyang Technological University (NTU), Singapore, where he is Cluster Director of Power Electronics at the Energy Research Institute at NTU (ERI@N) and co-Director of the Rolls-Royce at NTU Corporate Lab. From February 2001 to January 2002, and February 2005 to January 2006, he was a Researcher at the Center for Power Electronics Systems, Virginia Tech, Blacksburg. From January 2012 to January 2013, he was a Visiting Professor at the Australian Energy Research Institute, UNSW, Sydney. He has authored more than 380 published technical papers and has been involved in several industrial projects and educational programs in the fields of power electronics and systems. His research interests include modulation and control of power converters, multilevel converters, renewable energy, energy storage, power quality, HVdc transmission systems, and more-electrical aircraft and vessels.

He is Associate Editor of the *IEEE Journal of Emerging and Selected Topics in Power Electronics*. He was co-Editor-in-Chief and Associate Editor of the *IEEE Transactions on Industrial Electronics*. He received the 2018 IEEE Bimal Bose Award for Industrial Electronics Applications in Energy Systems.